AN IN-ROAD SENSING DEVICE FOR PAVEMENT HEALTH MONITORING USING INTERNET OF THINGS AND SIGNAL PROCESSING

AJ HOFFMAN and A FIORITA

School of Electrical, Electronic and Computer Engineering, North-West University, Private Bag X6001, 2520, Potchefstroom, South Africa

ABSTRACT

Continuous pavement health monitoring detects the early degradation of pavement structures and extends the lifetime thereof by informing predictive maintenance actions. The high cost of traditional pavement condition monitoring techniques however restricts the frequent use of conventional pavement condition assessment methods. Therefore, a need exists for a method that enables low cost, high coverage, and continuous monitoring of pavement structures. This paper presents the specification, design, development and testing of a low-cost wireless self-powered in-road sensing device that continuously assesses pavement condition and communicates outcomes to a central maintenance system. Unlike traditional systems, the proposed solution combines a suite of different sensors to provide valuable insight into all major factors that affect pavement health. Measurands, including the pavement deflection at the time of vehicular loading, temperature, humidity, and moisture content are captured at different layers of the pavement structure. Low-cost accelerometers accurately measure the acceleration of the pavement material, and an on-board processor converts this information to a compact set of pavement condition outcomes that are communicated to a hub using a LoRa sensor network that combines long read range, low power consumption and sufficient communication speed. A solar cell and battery provide continuous power to the system, allowing 24/7 operation even in dense traffic conditions. Our results demonstrate that the design objectives can be satisfied using affordable off-the-shelf electronic components, justifying practical deployment of this concept.

1. INTRODUCTION

Road networks, crucial for economic development and supply chain connectivity, suffer long-term structural decay due to environmental and daily loading conditions, particularly pronounced in South Africa. Poorly designed roads, subjected to excessive stress, result in multiple cracks and the formation of potholes (SANRAL, 2013). This necessitates costly corrective maintenance actions to meet the road's intended lifespan (SANRAL, 2013). For example, R81.1 billion was spent on the delivery and maintenance of South African roads in the year 2020 (National Treasury, 2021). Early degradation detection through continuous performance monitoring becomes essential for cost-effective interventions. Traditional systems, like Automated Pavement Condition Surveys (APCS) and Falling Weight Deflectometer (FWD) tests, prove impractical due to high costs, limited coverage, and traffic disruptions (Bajwa et al., 2020; Bahrani et al., 2020; Aceves, 2020). In contrast, wireless, self-powered in-situ measurement devices, present a viable solution (Shtayat et al., 2020; Barriera et al., 2020). This paper proposes such a wireless device, incorporating low-power in-situ sensors for comprehensive pavement assessment. Unlike prior studies, it wirelessly senses various parameters such as temperature and humidity, enhancing its novelty.

1.1 Aim of Paper

This project aims to develop a low-cost wireless in-road sensor for continuous monitoring of pavement behaviour under dynamic loading and real-world conditions without disrupting traffic. The device introduces the novelty of wireless operation, utilizing low-power in-situ sensors to offer a holistic view of pavement conditions,

1.2 Problem Statement

Unmanaged pavement deterioration causes significant maintenance costs. Excessive stresses, caused by overloaded vehicles, on poorly designed roads lead to multiple cracks, rutting, and the formation of potholes. Unroadworthy vehicles worsen this situation. Achieving road longevity requires costly corrective maintenance actions. Therefore, preventive solutions and early stress identification are crucial. Existing solutions (automated pavement condition survey, multi-depth deflectometer and falling weight deflectometer) fall short of effectively meeting this need. Therefore, there is a pressing need to enhance road health monitoring by increasing frequency and coverage of assessments while reducing costs.

1.3 Scope of Paper

The paper will detail the design of the in-road sensor device, implementation, and real-world in-road testing in different scenarions. It involves developing the sensing device, selecting wireless communication protocols, and optimizing data transmission to a central server. The approach is to convert measured pavement acceleration to displacement, and to compare the accuracy of inferred displacement with traditional methods, including the linear vertical displacement transducer (LVDT). Minimising cost and maximising power efficiency are design priorities. The study excludes the design of the core communication network and user interface. The ensuing sections cover pavement behaviour, device design, implementation, and real-world in-road testing, and conclude with future work.

2. RESPONSE OF THE PAVEMENT TO APPLIED LOADS

Under applied loads, the pavement undergoes deflection, resulting in the formation of an indentation referred to as a deflection bowl (SANRAL, 2013). Illustrated in Figure 1, this deflection bowl arises from the stress at the tire-pavement contact and is influenced by pavement structure properties like temperature, stiffness, and moisture content (García et al., 2017). Measurement of elastic deflection (which is reversible) allows for the back-calculation of pavement layer stiffness. Pavements can also experience permanent deformation, which is referred to as rutting. Both types of deformation are of interest for this study.

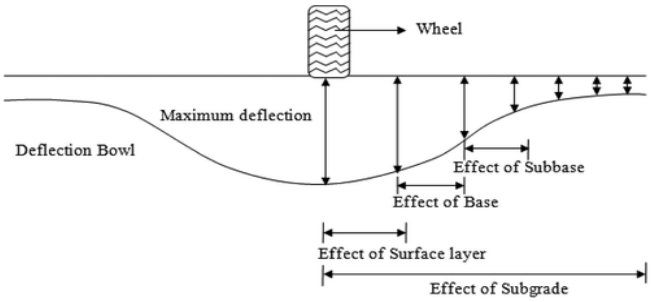

Figure 1: Deflection bowl created by a tire-pavement contact (Mosale Ramanath et al., 2020)

In addition to pavement deflection, other factors influence its condition:

Temperature: Elevated temperatures reduce the stiffness modulus, diminishing the pavement's resistance to damage (Meizhu Chen et al., 2010). Rutting which is common at high temperatures and high traffic volumes, can be addressed through a temperature profile of the pavement layers, guiding mitigation measures.

Moisture Content: The infiltration of moisture into the pavement surface weakens the bond between aggregate and bitumen layers, making the pavement susceptible to rutting (Omar et al., 2020). Assessing moisture content profiles identifies areas that are prone to excess moisture.

Humidity: Pavement humidity affects the stiffness modulus and rutting resistance, with higher humidity leading to increased deflections. Monitoring humidity profiles assist in pinpointing drainage issues within the structure.

3. DEVICE DESIGN

3.1 Device Architecture and Hardware Design

The device consists of five essential components namely, the power subsystem, sensors, communication subsystem, storage, and the processing unit as illustrated in Figure 2.

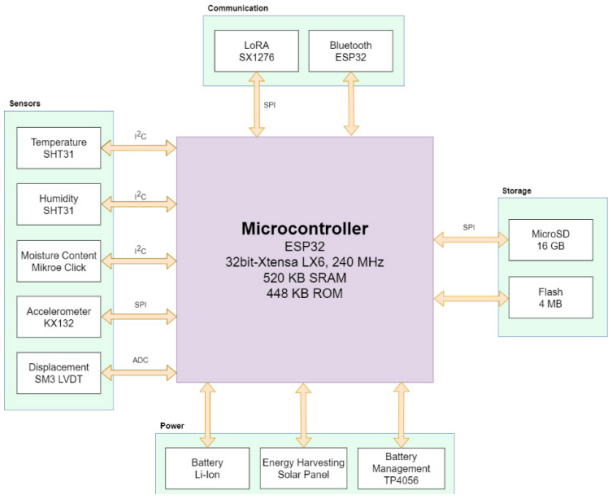

Figure 2: The architecture of the device

3.2 Processor

The microcontroller unit (MCU) is pivotal for data processing, interconnection, and software management, with the ESP32 microprocessor chosen for its balance between processing capabilities, cost, and power efficiency. The alternative microcontrollers considered were the ATmega328P, known for its widespread use in Arduino boards, offering simplicity and ease of use but lacking in processing power. The STM32L072CZ stands out for its low power consumption and extensive peripheral options, yet it does not provide built-in wireless communication capabilities and its availability is limited. Similarly, the RP2040, while boasting impressive processing power and versatile I/O options, does not offer integrated Bluetooth or Wi-Fi functionalities found in the ESP.

Sensors: Accurately assessing pavement conditions necessitates the following sensors to fulfil specific performance criteria:

Displacement Sensor:

- Accuracy - +/- 5 µm
- Range - +/- 1500 µm
- Frequency Response - Minimum 500 Hz

The LVDT is the conventional method to measure pavement deflection in a laboratory setup. Employing a +/- 3mm AC LVDT from Solartron alongside external signal conditioning, the displacement sensor gauges pavement deflection with a precision of +/- 7.5 µm, surpassing the specified accuracy. The bandwidth of the conditioning circuitry is 500 Hz, meeting the specified requirement.

As inroad pavement condition assessment requires low-cost and low-power sensing, LVDTs will only be used during the testing phase. Accelerometers, being smaller and more power-efficient, offer a viable alternative for operational inroad displacement sensing.

Accelerometer:

- Bandwidth – 0 Hz to 1 kHz
- Range - +/- 200 mg to +/- 1 g
- Resolution - Smaller than 500 µg
- Sensitivity - Larger than +/- 1 V/g

In this case g refers to the acceleration of gravity on earth ($9.8 m/s^2$) and not grams. The KX132 accelerometer satisfies all the aforementioned criteria and surpasses competing options. It incorporates on-chip digital signal processing, maintains a low current draw of 240 µA, and boasts a sufficient sampling rate of up to 25.6 kHz.

Temperature and Humidity Sensor:

- Accuracy - +/- 5 % RH, +/- 1 °C
- Range - 0 to 100 % RH, - 10 to 100 °C

The SHT31 humidity sensor guarantees exceptional accuracy (+/- 1.5 % RH) and surpasses temperature reading specifications (+/- 0.2 °C) over an extensive range (-40 to 90 °C). Housed in weather-proof casing, the sensor is ideally suited for direct integration into pavement material, perfectly aligning with our application needs.

Moisture Content Sensor:

- Accuracy - +/- 5 % per Volume
- Range - Larger than 5 % per Volume

While capacitive sensors are generally considered less precise than alternatives, they present advantages in terms of availability, cost-effectiveness, and size. The Hydroprobe Click is a cost-effective capacitive soil moisture content sensor with a compact form factor.

Wireless communications: Efficient power consumption is crucial for the communication protocol in large-scale deployments. A preferred choice is LoRaWAN due to its optimal balance between latency, power consumption, speed, and range. The SX1276 LoRa transceiver offers long range and low power usage.

Memory: To mitigate communication disruptions between the device and its gateway, a microSD slot with a 16 GB card is integrated, facilitating uninterrupted pavement data capture. With daily data volumes (500 KB, see section 5) in mind, this setup offers storage for over 90 years of information, ensuring data integrity and sustained monitoring.

Power: For wireless designs, effective energy management is crucial to extend device lifespan. Utilizing a rechargeable Li-Ion pack, the in-road sensor integrates a 500-mW solar panel charging a 500 mAh Li-Ion battery through a controller that includes temperature regulation and current monitoring.

3.3 Software Design

The software for the device consists of two components, the software running on the microcontroller and the software for the external processing of the data. The microcontroller software is written in the C/C++ language, which handles data collection (using I^2C and SPI serial peripheral interfaces), data processing, and data communication. Given the constrained data capacity of the LoRa link in the testing phase data is captured through the Bluetooth interface to a Personal Computer to enable the transmission of all raw measured data, facilitating detailed analysis of the accelerometer and LVDT data.

Converting accelerations to displacement through double integration poses challenges, amplifying baseline offsets and introducing low-frequency components (Bajwa et al., 2020). Correction methods, involving filtering, amplification, and detrending, are crucial for accurate displacement estimation. Figure 3 illustrates the strategy for converting acceleration to displacement. Firstly, the baseline drift is eliminated by fitting a second-order least-squares polynomial to the accelerometer data and subtracting it. Secondly, trapezoidal numeric integration is applied to derive velocity and displacement from the acceleration and velocity data, respectively. Equations (1) and (2) illustrate this integration, assuming a zero initial acceleration.

$$v(n) = \sum 0.5(a(n)+a(n+1))(\Delta t) \quad (1)$$

$$d(n) = \sum 0.5(v(n)+v(n+1))(\Delta t) \quad (2)$$

where a is the acceleration, v is the velocity, d is the displacement, and Δt is the time step in seconds, while n indicates the incremental time steps. Following the integration, the added low-frequency component and high-frequency noise are addressed. A band-pass Butterworth filter (2–40 Hz) is applied to remove undesired frequencies, and a Hilbert transform eliminates oscillatory behavior in the displacement estimate. Adjusting the filter's lower cut-off frequency is imperative with increasing vehicle speed (Bahrani et al., 2020).

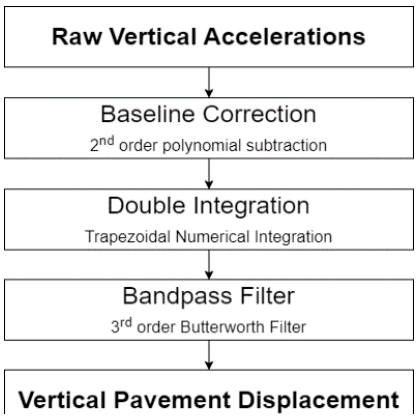

Figure 3: Converting acceleration to displacement

4. DEVICE IMPLEMENTATION

This section details the physical implementation of the aforementioned architecture. The system components mentioned above are all integrated into a printed circuit board (PCB).

Figure 4(a) displays the control card PCB, while Figure 4(b) depicts the power supply card, featuring inputs for the solar panel, battery, and current sensor, along with the charge controller and regulator (in blue).

(a) (b)

Figure 4: (a) The control card and (b) the power card

The PCB is housed in a PVC/PLA casing that is embedded in the pavement layers to a depth of 200mm as shown in Figure 5. The casing consists of a 3D-printed inner casing and an outer PVC casing, which adds additional structural support. Figure 5 shows the asphalt concrete (AC) layer and the unbound granular base (UGB) layer. It also depicts the placement of the accelerometer (Acc) and LVDT core on a U-shaped aluminium bracket. The LVDT core is connected at the centre of the bracket, sliding in the LVDT body, which is anchored at the bottom of the cavity. The sensors are placed at different depths in pavement material (typically one in the asphalt, one just below the asphalt and one in the based layer). The solar panel is integrated into the inner casing lid and shielded by a 5mm thick polycarbonate plate. The casing is depicted in Figure 6(a) and Figure 6(b), featuring a removable foot piece that facilitates the installation process.

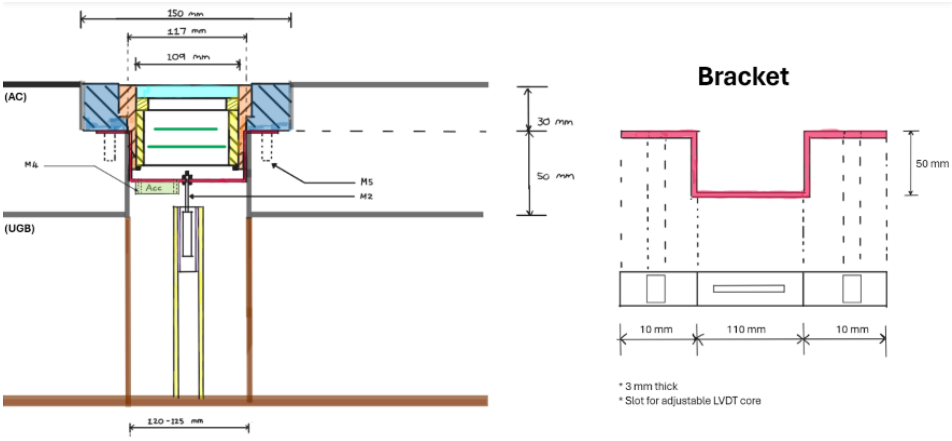

Figure 5: The design and placement of the device and its sensors

Figure 6: (a) The constructed casing (b) The removable foot piece

5. EXPERIMENTAL RESULTS AND DISPLACEMENT SENSOR CALIBRATION

Prior to the in-road testing phase, laboratory tests were conducted to calibrate the sensors. The Creality Ender 3 Pro 3D printer, with a layer resolution of 100 microns, served as a reference for accelerometer and LVDT displacement estimates. Controlled upward deflections were simulated by moving the printer head in the z-axis. Twenty repetitions at each of the five displacement values were recorded and analysed. The mean displacement measurements of the 1 mm deflections are presented in Figure 7.

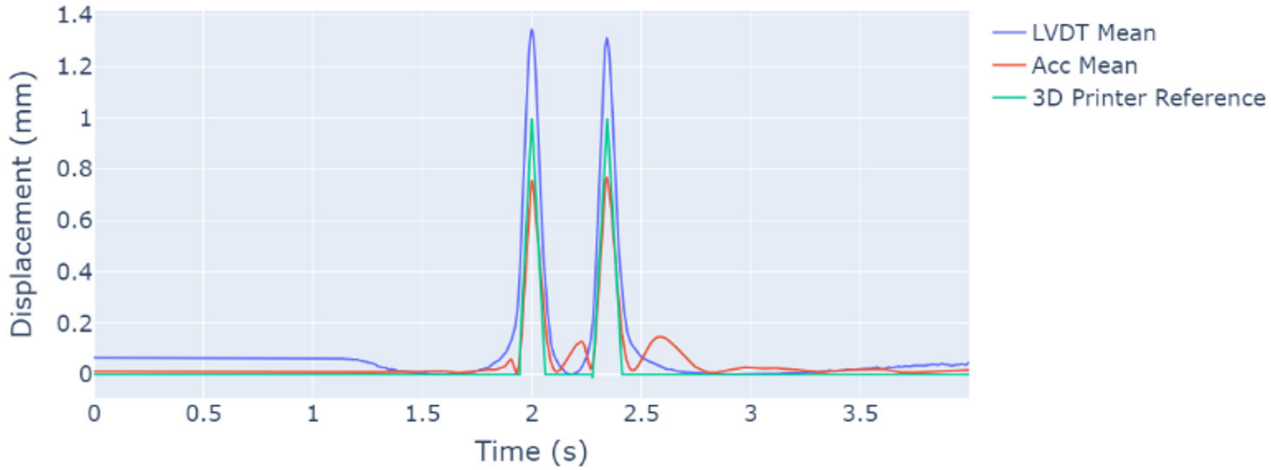

Figure 7: The mean of the LVDT and accelerometer measurements

The plots indicate that both accelerometer estimates and LVDT measurements align in the time axis but exhibit different amplitudes compared to the reference displacement. This amplitude difference in accelerometer estimates can be attributed to the filtering since a lower cut-off frequency fails to effectively suppress low-frequency noise, distorting the signal. Increasing the cut-off frequency enhances signal shape but reduces amplitude, necessitating post-filtering signal amplification (Bahrani et al., 2020). To calibrate results, a linear calibration equation is added to the resultant deflections for both sensors. This significantly improves the results as seen in Figure 8.

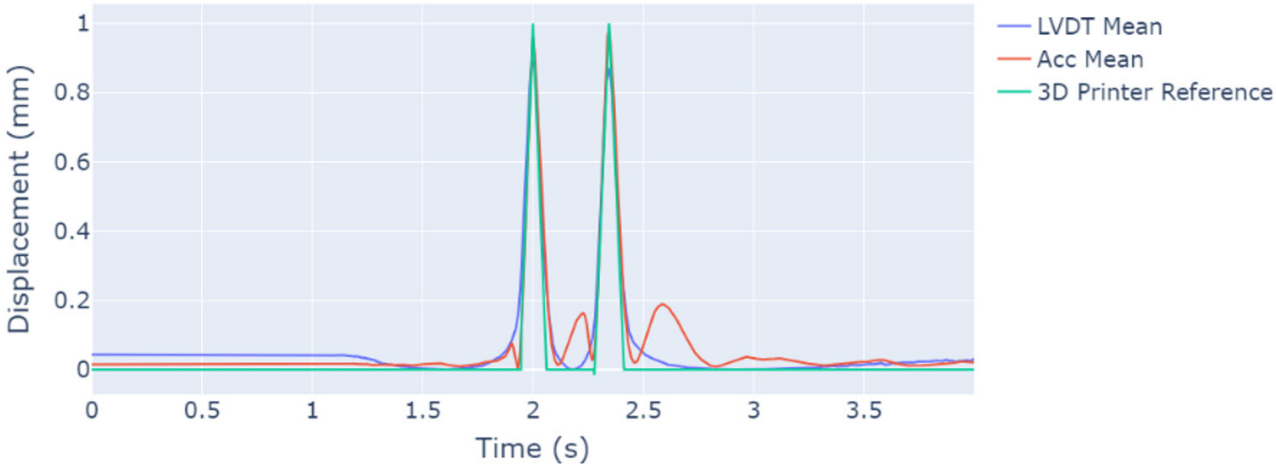

Figure 8: The calibrated accelerometer and LVDT estimates for a 1mm reference pulse

6. IN-ROAD TESTING

Figure 9 displays the device installed in a 200 mm deep, 150 mm diameter cavity. Tests cover three pavement types, measuring deflections at different speeds and with changing

lateral wheel-to-device distance. For each pavement type, ten repetitions were conducted at each speed and wheel-to-device distance. The results are averaged to obtain an overall pavement deflection measurement. Temperature, humidity, and moisture content tests are conducted solely in the initial test environment. Furthermore, the tests did not take the tyre pressure into account and is left as a future task.

(a) Top view (b) Side view

Figure 9: The installed in-road device

6.1 Thin Asphalt Layer

The asphalt layer for the first test is 40 mm thick and seated on compacted brown soil. The test vehicle that was used is a 2-tonne pick-up truck. The pavement deflected by an average of 521 µm (Accelerometer - Front Axle), 437 µm (Accelerometer - Rear Axle), 460 µm (LVDT - Front Axle), and 419 µm (LVDT – Rear Axle) across various speeds. Displacement as a function of speed is depicted in Figure 10 below. It is evident that the LVDT shows a consistently lower pavement deflection compared to the accelerometer, except at 60 km/h speeds. The average difference between the two sensors is 40 µm, partially explained by (Arraigada et al., 2008), attributing it to the accelerometer measuring the entire pavement structure's deflection, while the LVDT measures relative deflection between top and bottom layers. The LVDT's installation method, using a L-bracket fixated using screws, might also have led to the discrepancy. A slight decrease in pavement deflection is observed as the speed of the vehicle increases, aligning with findings in (Bahrani et al., 2020; Mshali & Steyn, 2020). This occurrence can be explained by the asphalt layer's behaviour under load. The modulus of elasticity of asphalt rise with higher loading rates, indicating increased resistance to deformation at faster vehicle speeds and resulting in smaller deflections. However, as this relationship is influenced by the properties of the pavement, this behaviour may not be the same for different pavement types as will be seen in the last test case.

Varying the lateral distance between the wheel and the device demonstrates sensor sensitivity and the deflection bowl discussed in Chapter 2. In Figure 11, the accelerometer consistently shows higher deflection than the LVDT when the wheel's centre is near the device. The deflection bowl shape aligns with practical findings, but device sensitivity limits the detection distance. The accelerometer detects deflection up to 15cm, with an estimated bowl radius of approximately 64cm. The LVDT, less sensitive, detects deflection only up to 10cm. Device sensitivity limit the distance of detectable deflections for both devices.

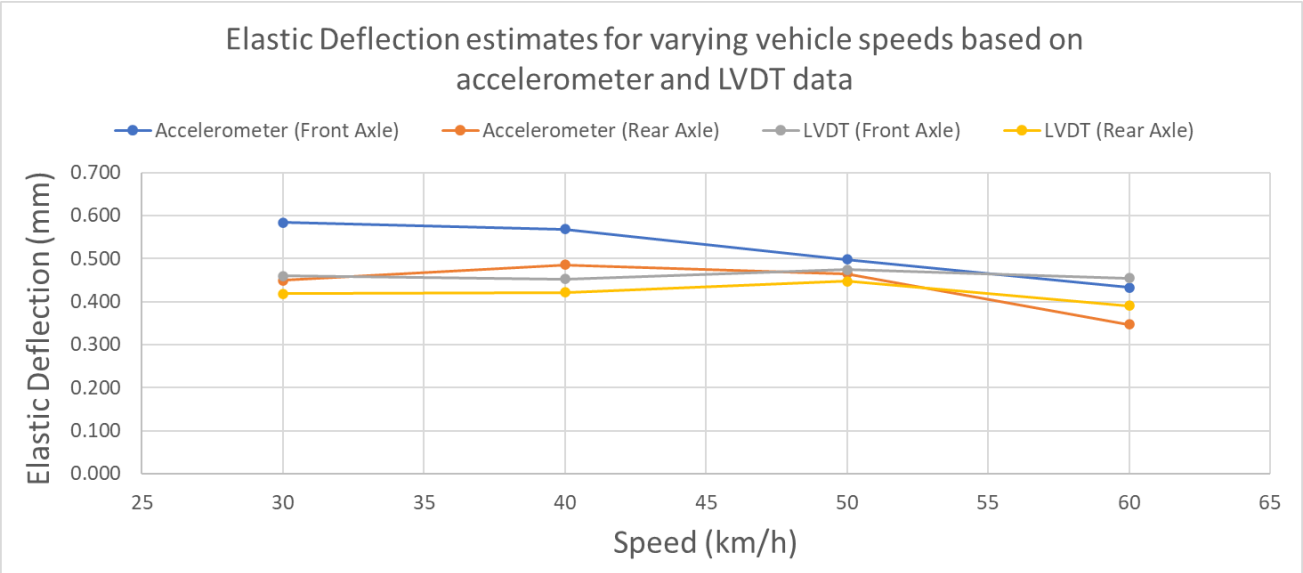

Figure 10: The deflection of a 40 mm AC layer for varying vehicle speed

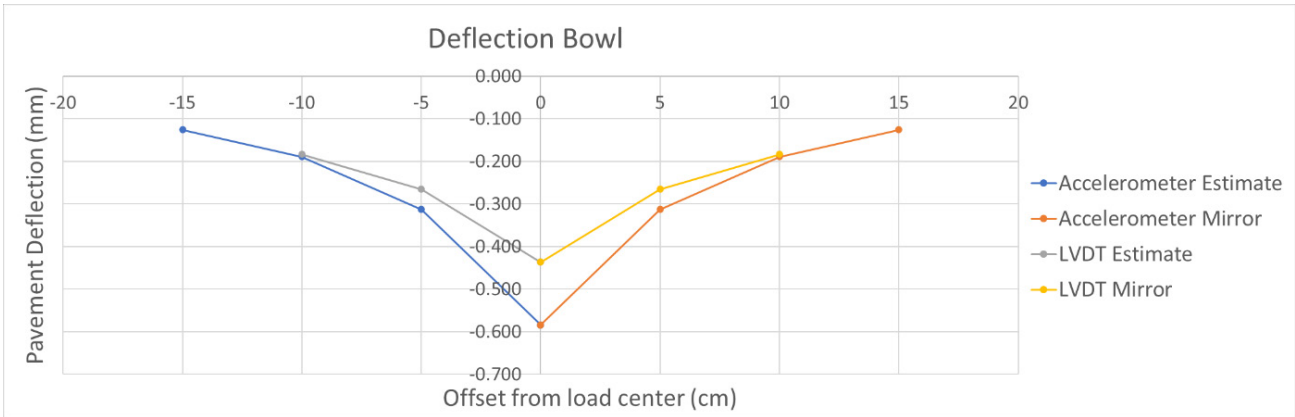

Figure 11: The pavement deflection as the wheel-to-sensor distance changes

6.2 Medium Thickness Asphalt Layer

This test section comprises an 80 mm thick asphalt concrete layer atop a granular base layer, with a 10-tonne road rail vehicle (RRV) as the test vehicle. Figure 12 displays measured deflection for front and rear axles. The front wheel induces a more significant pavement deflection despite the rear wheels applying a greater downward force, due to a double wheelset on each side of the rear axle. The reference instrument used was a light-weight deflectometer (LWD). Good correlation between deflection estimations from the accelerometer and the LWD was observed. The accelerometer recorded an average deflection of 278 µm across various speeds, while the LWD registered an average of 178 µm, as it exerted 6 kN less than the RRV.

6.3 Thick Asphalt Layer

In the test on the N4 section with a 200 mm thick asphalt layer atop a granular base layer, the RRV speed could be increased to 60 km/h, yielding an accelerometer-estimated average deflection of 204 µm and a significant spike at 60 km/h as seen in Figure 13. This is markedly higher than the reference measurement average of 50 µm, resulting in a notable estimation error. The LVDT, while showing a more consistent deflection, exhibits a significantly higher amplitude than the LWD. Possible reasons include the asphalt

concrete layer construction or variations in the types of force exerted by the LWD compared to an actual driving vehicle. Additionally, the calibration offset limits the sensor's precision at very low deflection levels.

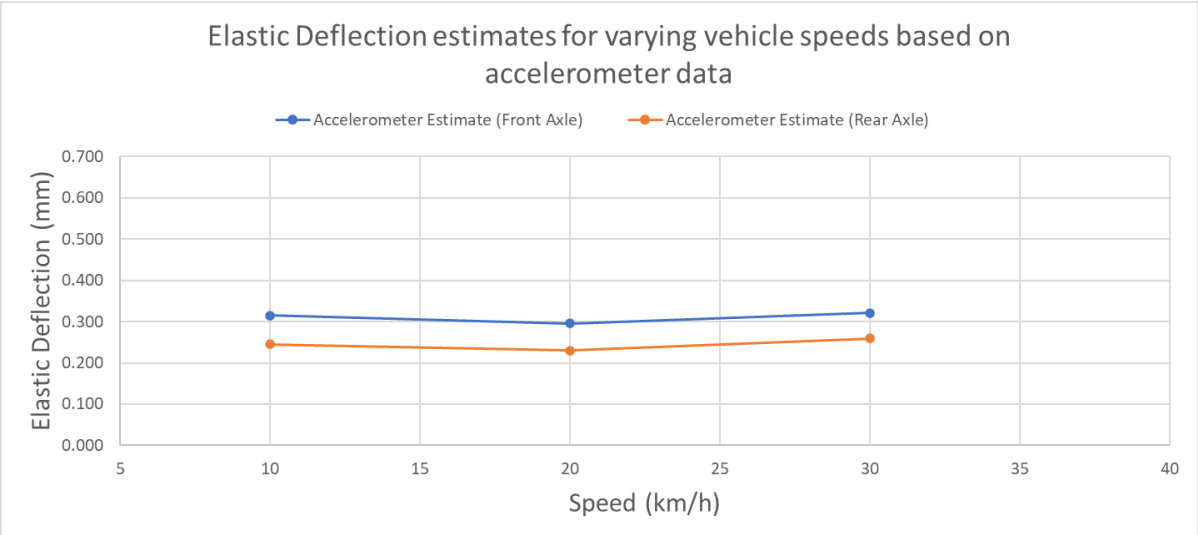

Figure 12: The pavement deflection with varying speed on a 80 mm thick AC layer

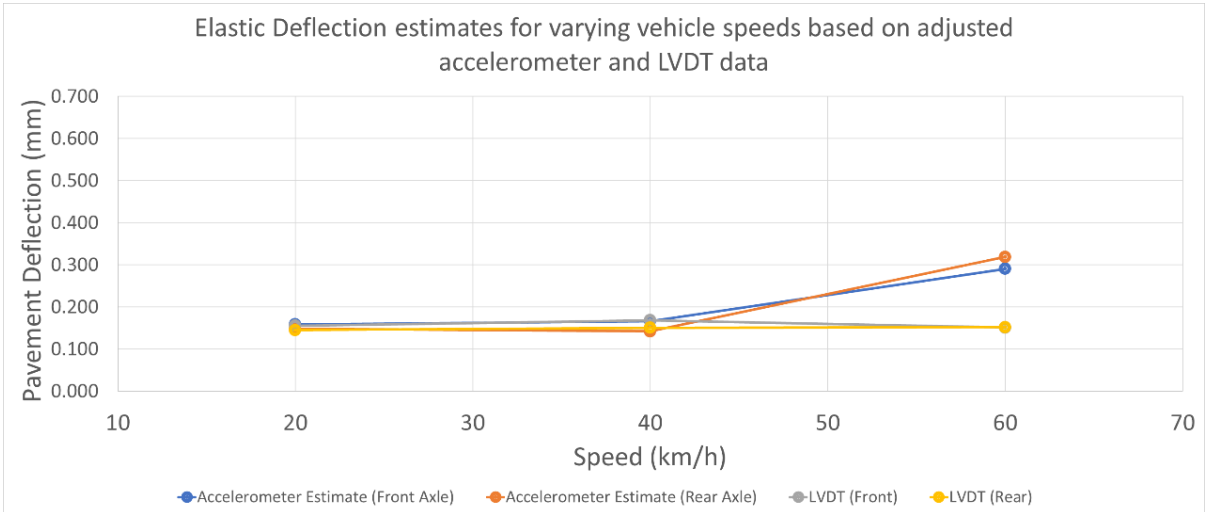

Figure 13: Deflection of a 200 mm asphalt layer at varying vehicle speed

6.4 Temperature Profile

A temperature profile of the pavement at different depths enables experts to evaluate potential damage, providing insights into pavement design, material properties, and necessary preventive maintenance measures. The temperature profile illustrated in Figure 14, obtained at a depth of 10cm, reveals a maximum of 19.78°C at midday and a minimum of 14.3°C in the early morning. Night time temperatures were not recorded. Additionally, the ambient temperature is shown, with an average difference (ΔT) of 2.7°C compared to the pavement temperature.

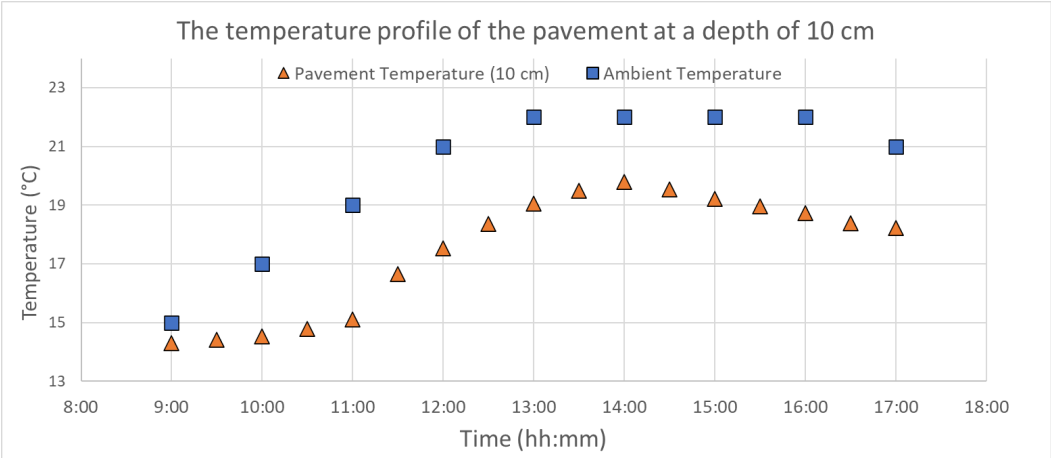

Figure 14: The temperature profile at 10 cm

6.5 Humidity Profile

Humidity influences moisture absorption within pavement layers, with elevated humidity correlating to increased absorption. This, in turn, impacts properties like pavement stiffness. Figure 15 reveals a relatively constant humidity value throughout the day, with a maximum decrease of 0.31 % in humidity levels at warmer temperatures. The high humidity levels can be attributed to the rainy weather prior to the measurements.

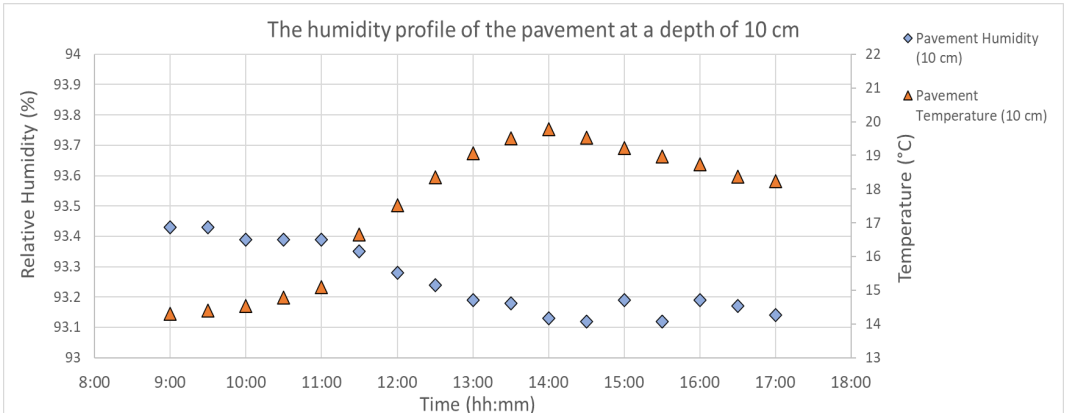

Figure 15: The humidity profile at 10 cm

6.6 Moisture Content Profile

Similar to humidity levels, elevated moisture content diminishes the load-bearing capacity of the pavement. Figure 16 illustrates the humidity levels at a 5 cm depth in the pavement, revealing a slight uptick in moisture content during the hours between 12:00 and 14:00.

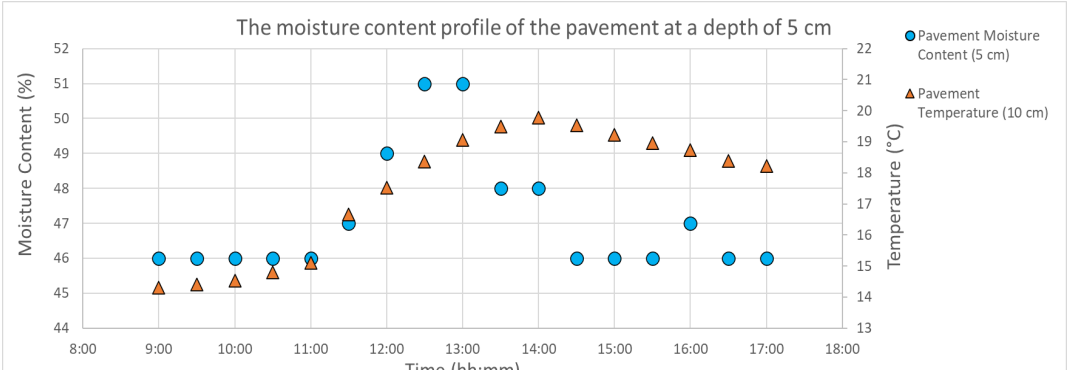

Figure 16: The moisture content profile at 5 cm

6.7 Communication System

The communication subsystem requires a message transmission for each passing vehicle. Key factors influencing packet transmission rate include bandwidth, coding rate, spreading factor, and packet construction. For instance, a spreading factor of 12, bandwidth of 125 kHz, coding rate of 1, and payload length of 51 bytes results in a 2.5-second time on air. In contrast, a spreading factor of 7, bandwidth of 250 kHz, coding rate of 1, and the same payload length yields a faster 50 milliseconds but restricts communication range.

For the in-road device, a 5-byte payload, including a 2-byte displacement estimate and 3-byte timestamp, transmitted with a spreading factor of 7, bandwidth of 125 kHz, and coding rate of 1, takes 30 milliseconds. At speeds around 100 km/h, the LoRa subsystem cannot transmit between consecutive axles. Implementing a buffer system that transmits data once all axles were captured resolves this issue, improving transmission efficiency.

The LoRa subsystem's required transmission capacity is determined by calculating the daily data generated by the device (deflection, profile measurements, and system status), yielding just over 500 KB as shown in Table 1. This includes 50,000 deflection measurements based on expected maximum traffic flow per day (Hoehler, 2017), 24 hourly profile measurements, and 24 status updates per day.

Table 1: Daily data amount generated by the in-road device

Source of data	Bytes Required	Number of measurements	Total Bytes generated
Pavement deflection measurement	5	100000	500000
Temperature, Humidity and Moisture Content measurement	7	24	168
System Status Byte	4	24	96
Total	16	100048	500264

To ascertain the LoRa subsystem's capability to manage this data volume, an examination of the duty cycle limit is necessary. The 868 MHz frequency band imposes a duty cycle limit of 1%. Employing an online LoRa duty cycle calculator reveals an allowable data transmission size of approximately 508 KB per day, which satisfies the requirement.

6.8 Power Consumption

The device's energy consumption (E_{daily}) is determined by equation (3), with $P_{n(effective)}$ representing the average daily power in watts and t_{on} indicating the active time per day. Average power (P) is calculated according to equation (4), factoring in device voltage (V), run current (I_{run}), active time fraction (T_{run}), standby current (I_{idle}), and idle time fraction (T_{idle}).

$$E_{daily} = P_{n\,(effective)} t_{on} \tag{3}$$

$$P_{(effective)} = V(I_{run}T_{run} + I_{idle}T_{idle}) \tag{4}$$

A comprehensive breakdown of each component's energy consumption is provided in Table 2. The table does not include component duty cycles, which determine the active and sleep times. Sensors for temperature and humidity read hourly, while the accelerometer runs continuously. Assuming 50,000 vehicles on the freeway per day, the ESP32 is active around 250 minutes, and LoRa operates just under its 1% duty cycle, requiring about 14.5 minutes of daily active transmission. The device's daily consumption is 1,071 mWh. Solar production peaks at mid-day, generating a total of 1,964 mWh per day, ensuring sufficient power for battery replenishment.

Table 2: The daily energy consumption of the components of the device

	$P_{effective}$ (mW)	Daily Consumption (Wh[A1][A2])
Accelerometer	6.600	0.158
Humidity and Temperature sensor	0.252	0.006
Moisture content sensor	3.300	0.079
LoRa	2.263	0.05[A3][A4]4
ESP32 (@80 MHz)	32.218	0.773

7. CONCLUSIONS AND FUTURE WORK

This paper describes a wireless in-road device for pavement condition monitoring that surpasses traditional systems in terms of cost, coverage, and assessment frequency. The embedded solution allows continuous, real-time data collection, offering uninterrupted assessment of road functionality. The accuracy of the overall system in real-world conditions was assessed, demonstrating reliable temperature and humidity measurements but highlighting challenges in pavement deflection estimates, especially in stiffer pavement structures. Challenges with accelerometer-based deflection measurements were identified, requiring speed-dependent calibration. Future research directions include hardware revision, comprehensive software integration, speed-based filter adjustments, investigation of deflection anomalies, enhanced moisture content measurement, and testing the ability of the sensor to accurately assess permanent pavement damage, including cracking and rutting.

8. REFERENCES

Aceves, S. 2020. Automated Pavement Condition Survey (APCS), [Online]. Available at: https://catc.ca.gov/-/media/ctc-media/documents/ctc-workshops/2020/06/202006-apcs-presentation.pdf. Accessed 19 January 2024.

Arraigada, M et al. 2008. Evaluation of accelerometers to determine pavement deflections under traffic loads, *Materials and Structures*, 42(6):779-790. Doi: 10.1617/s11527-008-9423-5.

Bahrani, N et al. 2020. Alternate method of pavement assessment using geophones and accelerometers for measuring the pavement response, *Infrastructures*, 5(3):25. Doi: 10.3390/infrastructures5030025.

Bajwa, R et al. 2020. Pavement performance assessment using a cost-effective wireless accelerometer system, Computer-Aided Civil and Infrastructure Engineering, 35(9):1009-1022. Doi: 10.1111/mice.12544.

Barriera, M et al. 2020. In situ pavement monitoring: A Review, *Infrastructures*, 5(2):18. Doi: 10.3390/infrastructures5020018.

García, Á et al. 2017. Wireless monitoring of pavement temperature based on low cost computing platform, The 4th International Electronic Conference on Sensors and Applications [Preprint]. Doi: 10.3390/ecsa-4-04903.

Hoehler, CA. 2017. Traffic loading on the greater Johannesburg municipal road network, unpublished.

Meizhu Chen et al. 2010. High-temperature hazards and prevention measurements for asphalt pavement, 2010 International Conference on Mechanic Automation and Control Engineering [Preprint]. Doi: 10.1109/mace.2010.5536275.

Mosale Ramanath, A et al. 2020. Benchmarking falling weight deflectometer deflection bowl parameters: Case study for Indian conditions and the applications to rehabilitation design, *Journal of Transportation Engineering, Part B: Pavements*, 146(3). Doi: 10.1061/jpeodx.0000204.

Mshali, MR & Steyn, W JvdM. 2020a. Effect of truck speed on the response of flexible pavement systems to traffic loading, *International Journal of Pavement Engineering*, 23(4):1213-1225. Doi: 10.1080/10298436.2020.1797733.

Local Government Budgets and Expenditure Review. 2021. Publications – Inter-governmental Fiscal Reviews (IGFR) - 2021 [Preprint]. Available at: https://www.treasury.gov.za/publications/igfr/2021/prov/Chapter%207%20-%20Roads%20and%20Transport.pdf. Accessed 19 January 2024.

Omar, HA et al. 2020. Effects of moisture damage on asphalt mixtures, *Journal of Traffic and Transportation Engineering* (English Edition), 7(5):600-628.
Doi: 10.1016/j.jtte.2020.07.001.

Shtayat, A et al. 2020. A review of monitoring systems of pavement condition in paved and unpaved roads, *Journal of Traffic and Transportation Engineering* (English Edition), 7(5):629-638. Doi:10.1016/j.jtte.2020.03.004.

South African National Roads Agency Limited (SANRAL). 2013. South African Pavement Engineering Manual, 1st ed. Gauteng, South Africa: SANRAL Ltd., pp. 1-20.